

Central exclusive diffractive production of two-pions from continuum and decays of resonances in the Regge-eikonal model

R.A. Ryutin ^{a,1}

¹NRC “Kurchatov Institute” - Institute for High Energy Physics, Protvino 142 281, Russia

Abstract Calculations of central exclusive diffractive production (CEDP) of two pions via continuum and resonance mechanism are presented in the Regge-eikonal approach. Data from STAR, ISR, CDF and CMS were analysed and compared with theoretical description. Preliminary extraction of $f_0(500)$, $f_0(980)$ and $f_2(1270)$ couplings to Pomeron, and also ρ meson contribution from photoproduction mechanism to the CEDP cross-section are considered. We show possible nuances and problems of calculations and prospects of investigations at present and future hadron colliders.

PACS 11.55.Jy Regge formalism · 12.40.Nn Regge theory, duality, absorptive/optical models · 13.85.Ni Inclusive production with identified hadrons · 13.85.Lg Total cross sections

Introduction

In previous papers [1],[2] general properties and calculations of the Central Exclusive Diffractive Production (CEDP) were considered. It was shown, especially in [2], that diffractive patterns (differential cross-sections) of CEDP play significant role in model verification.

In [3] we considered the low mass CEDP (LM CEDP) with production of two pion continuum. Here we expand this analysis and add contributions from CEDP of $f_0(500)$, $f_0(980)$, $f_2(1270)$ and exclusive vector meson photoproduction (EVMP) of ρ_0 meson to this process, taking into account also the interference between continuum and resonance mechanisms.

CEDP of two pions is one of the basic “standard candles” for LM CEDP. Why do we need exact calculations and predictions for this process?

- Di-pion LM CEDP is the tool for the investigation of hadronic resonances (like f_2 or f_0), since one of the basic hadronic decay modes for these resonances is the two pion one. We can extract different couplings of these resonances to reggeons (Pomeron, Odderon etc) to understand their nature (structure and the interaction mechanisms).
- We can use LM CEDP to fix the procedure of calculations of “rescattering” (unitarity) corrections. In the case of di-pion LM CEDP there are several kinds of corrections, in the proton-proton, pion-proton and also pion-pion channels.
- The pion is the most fundamental particle in the strong interactions, and LM CEDP gives us a powerful tool to go deep inside its properties, especially to investigate the form factor and scattering amplitudes for the off-shell pion.
- LM CEDP has rather large cross-sections. It is very important for an exclusive process, since in the special low luminosity runs (of the LHC) we need more time to get enough statistics.
- As was proposed in [3],[4], it is possible to extract some reggeon-hadron cross-sections. In the case of single and double dissociation it was the Pomeron-proton one. Here, in the LM CEDP of the di-pion we can analyze properties of the Pomeron-Pomeron to pion-pion exclusive cross-section.
- Diffractive patterns of this process are very sensitive to different approaches (subamplitudes, form factors, unitarization, reggeization procedure), especially differential cross-sections in t and ϕ_{pp} (azimuthal angle between final protons), and also $M_{\pi\pi}$ dependence. That is why this process is used to verify different models of diffraction.
- All the above items are additional advantages provided by the LM CEDP of two pions, which has usual properties of CEDP: clear signature with two

^ae-mail: Roman.Rioutine@cern.ch

final protons and two large rapidity gaps (LRG) [5],[6] and the possibility to use the “missing mass method” [7].

Processes of the LM CEDP were calculated in some other works [8]-[18] which are devoted to most popular models for the LM CEDP of di-mesons, where authors have considered phenomenological, nonperturbative, perturbative and mixed approaches in Reggeon-Reggeon collision subprocess. Nuances of some approaches were analysed in the introduction of [3].

In this article we consider the case, depicted in Fig. 1, and show how it can describe the data from ISR [19], [20], STAR [21]-[26], CDF [27],[28], CMS [29]-[31] collaborations.

In the first part of the present work we introduce the framework for calculations of double pion LM CEDP (kinematics, amplitudes, differential cross-sections) in the Regge-eikonal approach, which was considered in details in [3]. Here we take reggeized full (RF) case from four approaches of [3] which is the best in the data description.

Also we discuss some nuances of the calculations, which we should take into account in further more accurate analysis (elastic amplitudes for virtual particles, off-shell pion form factor, pion-pion elastic amplitude at low energies, nonlinearity of the pion trajectory, tensorial couplings and spin effects).

In the second part we analyse the experimental data on the process at different energies, extract some couplings of resonances to Pomeron, find the best approach and make some predictions for LHC experiments.

To avoid complicated expressions in the main text, all the basic formulae are placed to Appendixes.

1 General framework for calculations of LM CEDP

LM CEDP is the first exclusive two to four process which is driven basically by the Pomeron-Pomeron fusion subprocess. It serves as a clear process for investigations of resonances like $f_0(500)$, $f_0(980)$, $f_2(1270)$ and others with masses less than 3 GeV. At the moment, for low central di-pion masses it is a huge problem to use perturbative approach, that is why we apply the Regge-eikonal method for all the calculations. For proton-proton and proton-pion elastic amplitudes we use the model of [32], [33], which describe all the available experimental data on elastic scattering. For EVMP we use the similar model [34].

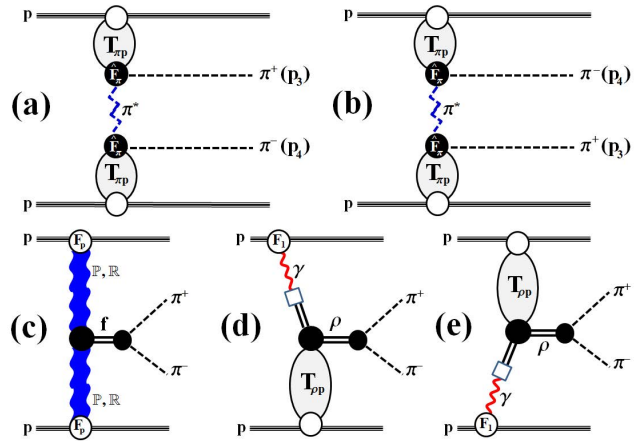


Fig. 1 Primary amplitudes (absorptive corrections are not shown) of the process of double pion LM CEDP $p + p \rightarrow p + \pi^+ + \pi^- + p$ in the Regge-eikonal approach for continuum (a),(b), LM CEDP of f_0 and f_2 resonances (c) and EVMP of ρ_0 meson (d),(e) with subsequent decay to $\pi^+\pi^-$. (a),(b): central part of the diagram is the primary continuum CEDP amplitude, where $T_{\pi^{\pm}p}$ are full elastic pion-proton amplitudes, and the reggeized off-shell pion propagator depicted as dashed zigzag line. This is the most applicable case from four approaches considered in [3]. (c): central part of the diagram contains Pomeron-Pomeron fusion with subsequent decay to pions, propagator is taken in the Breit-Wigner approximation. (d),(e): central part of the diagram contains full EVMP amplitude with ρ_0 production and decay. Off-shell pion form factor on (a),(b) and other suppression form-factors (in the Pomeron-Pomeron-f or the pion-pion- $(f_0, f_2, \rho_0$ vertices)) on (c),(d),(e) are presented as a black circles.

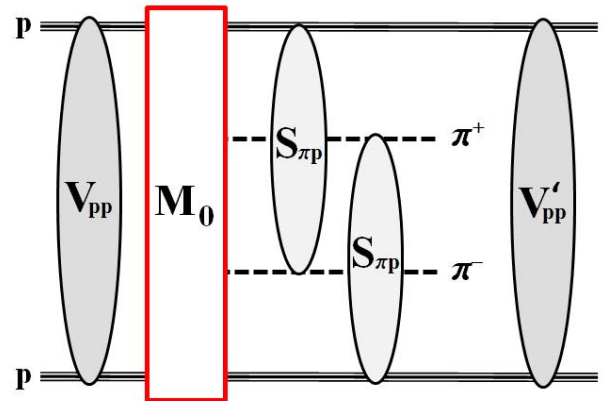


Fig. 2 Full unitarized amplitude of the process of double pion LM CEDP $p + p \rightarrow p + \pi^+ + \pi^- + p$. Proton-proton rescatterings in the initial and final states are depicted as V_{pp} and V'_{pp} -blobs correspondingly, and pion-proton rescattering corrections are also shown as $S_{\pi p}$ -blobs. Sum of primary amplitudes M_0 from Fig. 1 are shown as a red rectangle.

1.1 Components of the framework

LM CEDP process can be calculated in the following scheme (see Fig. 1):

1. We calculate the primary amplitudes of the processes, which are depicted as central parts of diagrams in Fig. 1. Here we consider the case, where the bare off-shell pion propagator in the amplitude for continuum di-pion production is replaced by the reggeized one

$$\mathcal{P}_\pi(\hat{s}, \hat{t}) = \left(\text{ctg} \frac{\pi \alpha_\pi(\hat{t})}{2} - i \right) \cdot \frac{\pi \alpha'_\pi}{2 \Gamma(1 + \alpha_\pi(\hat{t}))} \left(\frac{\hat{s}}{s_0} \right)^{\alpha_\pi(\hat{t})}, \quad (1)$$

where \hat{s} is the di-pion mass squared and \hat{t} is the square of the momentum transfer between a Pomeron and a pion in the Pomeron-Pomeron fusion process (see Appendix A for details).

In the present calculations we use linear pion trajectory $\alpha_\pi(\hat{t}) = 0.7(\hat{t} - m_\pi^2)$. Nonlinear case was also verified, and the difference in the final result is not significant.

We use also full eikonized expressions for proton-proton, pion-proton and photon-proton amplitudes, which can be found in the Appendix B.

2. After the calculation of the primary LM CEDP amplitudes we have to take into account all possible corrections in proton-proton and proton-pion elastic channels due to the unitarization procedure (so called “soft survival probability” or “rescattering corrections”), which are depicted as V_{pp} , V'_{pp} and $S_{\pi p}$ blobs in Fig. 1. For proton-proton and proton-pion elastic amplitudes we use the model of [32], [33] (see Appendix B). Possible final pion-pion interaction is not shown in Fig. 1, since we neglect it in the present calculations.

In this article we do not consider so called “enhanced” corrections [8]-[10], since they give nonleading contributions in our model due to smallness of the triple Pomeron vertex. Also we have no possible absorptive corrections in the pion-pion final elastic channel, since the central mass is low, and also there is a lack of data on this process to define parameters of the model. Nevertheless one can consider these corrections, as it was done by some authors recently [35], since they could play significant role for masses less than 1 GeV.

Exact kinematics of the two to four process is outlined in Appendix A.

Here we use the model, presented in Appendix B for example. You can use another one, which is proved to describe well all the available data on proton-proton, proton-pion elastic processes and exclusive ρ_0 photo-production. But it is difficult to find now more than a couple of models which have more or less predictable power (see [36] for detailed discussion). That is why we

use the model, which is proved to be good in data fitting, especially in the kinematical region of our interest.

1.2 Continuum di-pion production

Final expression for the amplitude for the continuum di-pion production with proton-proton and pion-proton “rescattering” corrections (see Fig. 1(a),(b)) can be written as

$$\begin{aligned} M^U(\{p\}) &= \\ &= \int \int \frac{d^2 \vec{q}}{(2\pi)^2} \frac{d^2 \vec{q}'}{(2\pi)^2} \frac{d^2 \vec{q}_1}{(2\pi)^2} \frac{d^2 \vec{q}_2}{(2\pi)^2} V_{pp}(s, q^2) V_{pp}(s', q'^2) \\ &\times [S_{\pi-p}(\tilde{s}_{14}, q_1^2) M_0(\{\tilde{p}\}) S_{\pi+p}(\tilde{s}_{23}, q_2^2) + (3 \leftrightarrow 4)] \quad (2) \\ M_0(\{p\}) &= \\ &= T_{\pi^+p}^{el}(s_{13}, t_1) \mathcal{P}_\pi(\hat{s}, \hat{t}) \left[\hat{F}_\pi(\hat{t}) \right]^2 T_{\pi^-p}^{el}(s_{24}, t_2), \quad (3) \end{aligned}$$

where functions are defined in (26)-(30) of Appendix B, and sets of vectors are

$$\{p\} \equiv \{p_a, p_b, p_1, p_2, p_3, p_4\} \quad (4)$$

$$\begin{aligned} \{\tilde{p}\} \equiv \{p_a - q, p_b + q; p_1 + q' + q_1, \\ p_2 - q' + q_2, p_3 - q_2, p_4 - q_1\}, \quad (5) \end{aligned}$$

and

$$\tilde{s}_{14} = (p_1 + p_4 + q')^2, \quad \tilde{s}_{23} = (p_2 + p_3 - q')^2, \quad (6)$$

$$s_{ij} = (p_i + p_j)^2, \quad t_{1,2} = (p_{a,b} - p_{1,2})^2, \quad (7)$$

$$\hat{s} = (p_3 + p_4)^2, \quad \hat{t} = (p_a - p_1 - p_3)^2 \quad (8)$$

Off-shell pion form factor is equal to unity on mass shell $\hat{t} = m_\pi^2$ and taken as exponential

$$\hat{F}_\pi = e^{(\hat{t} - m_\pi^2)/\Lambda_\pi^2}, \quad (9)$$

where $\Lambda_\pi \sim 1.2$ GeV is taken from the fits to LM CEDP of two pions at low energies (see next section). In this paper we use only exponential form, but it is possible to use other parametrizations (see [8]-[18]). Exponential one shows more appropriate results in the data fitting.

Other functions are defined in Appendix B. Then we can use the expression (17) to calculate the differential cross-section of the process.

1.3 CEDP and EVMP of low mass resonances.

For $f_0(500)$, $f_0(980)$, $f_2(1270)$ and ρ_0 resonances the general unitarized amplitude (see Fig. 1(c),(d)) is similar to the expression (2), where amplitude $M_0(\{p\})$ is replaced by the corresponding central primary amplitude for the resonance production and further decay to $\pi^+\pi^-$.

For f mesons amplitudes are constructed from proton-Pomeron form-factors, Pomeron-Pomeron couplings to mesons¹, off-shell propagators, off-shell form-factors and decay vertices.

For the EVMP amplitude of ρ_0 meson we take the full unitarized photon-proton amplitude contracted with the photon flux, and also with the off-shell meson propagator, off-shell form-factors and its decay vertex to pions. Also we have to sum this amplitude with the symmetric one with $t_1 \leftrightarrow t_2$.

All the primary amplitudes are presented in the Appendix C.

1.4 Nuances of calculations.

In the next section one can see that there are some difficulties and puzzles in the data fitting, which have also been presented in other works [11]-[18]. In this subsection let us discuss some nuances of calculations, which could change the situation.

We have to pay special attention to amplitudes, where one or more external particles are off their mass shell. The example of such an amplitude is the pion-proton one $T_{\pi+p}$ ($T_{\pi-p}$), which is the part of the CEDP amplitude (see (2)). For this amplitude in the present paper we use Regge-eikonal model with the eikonal function in the classical Regge form. And “off-shell” condition for one of the pions is taken into account by additional phenomenological form factor $\hat{F}_\pi(\hat{t})$. But there are at least two other possibilities.

The first one was considered in [38]. For amplitude with one particle off-shell the formula

$$T^*(s, b) = \frac{\delta^*(s, b)}{\delta(s, b)} T(s, b) = \frac{\delta^*(s, b) e^{2i\delta(s, b)} - 1}{2i} \quad (10)$$

was used. In our case

$$\begin{aligned} \delta(s, b) &= \delta_{\pi p}(s, b; m_\pi^2, m_\pi^2, m_p^2, m_p^2), \\ \delta^*(s, b) &= \delta_{\pi p}^*(s, b; \hat{t}, m_\pi^2, m_p^2, m_p^2) \\ \delta_{\pi p} &= \delta_{\pi p}^* \Big|_{\hat{t} \rightarrow m_\pi^2}. \end{aligned} \quad (11)$$

$\delta_{\pi p}$ is the eikonal function (see (22)). This is similar to the introduction of the additional form factor, but in a more consistent way, which takes into account the unitarity condition.

The second one arises from the covariant reggeization method, which was considered in the Appendix C

¹Here we take the simple scalar one for every meson, even for $f_2(1270)$ (multiplied by the leading tensor term), although, as was mentioned in our work [37], this vertex can be rather complicated and can give nontrivial contribution to the dependence on the azimuthal angle between final protons. But for our goals in this paper, namely, investigation of the di-pion mass distributions, it is rather good approximation.

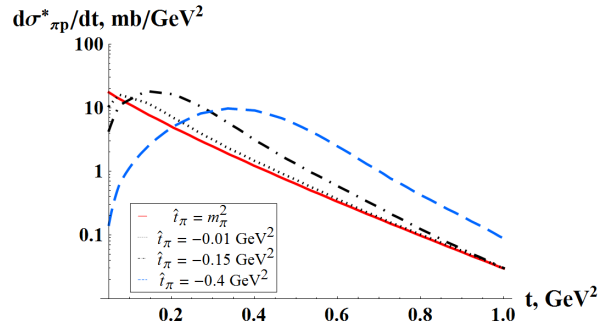


Fig. 3 Pion-proton on-shell and off-shell elastic differential cross-section (in the model of conserved meson currents presented in Appendix C) for different pion virtualities \hat{t}_π : m_π^2 (on-shell), -0.01 GeV^2 , -0.15 GeV^2 , -0.4 GeV^2 in the covariant approach with conserved currents.

of [3]. For the case of conserved hadronic currents we have definite structure in the Legendre function, which is transformed in a natural way to the case of the off-shell amplitude. But in this case off-shell amplitude has a specific behaviour at low t values (see Fig. 3 and [2] for details). As was shown in [2], unitarity corrections can mask this behavior.

Since final pion-proton interactions can give rather large suppression (about 10-20%, as in Fig. 4), in our calculations we use the full amplitude as depicted in Fig. 2.

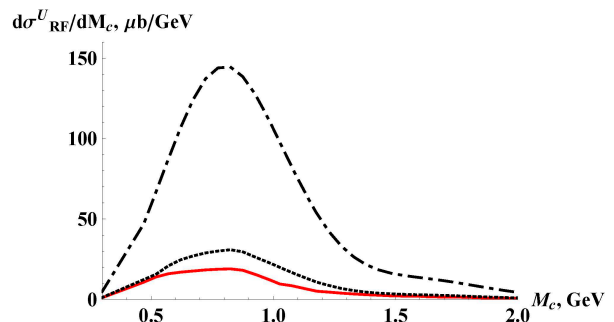


Fig. 4 Predictions of the model for the continuum (see Fig. 1(a),(b)) at 7 TeV. Curves from up to down correspond to the Born term, the amplitude with proton-proton rescattering corrections only and the one with all the corrections (proton-proton and pion-proton). $\Lambda_\pi = 1.2 \text{ GeV}$.

2 Data from hadron colliders versus results of calculations

Our basic task is to extract the fundamental information on the interaction of hadrons from different cross-sections (“diffractive patterns”):

- from t-distributions we can obtain size and shape of the interaction region;
- the distribution on the azimuthal angle between final protons gives quantum numbers of the produced system (see [2],[37] and references therein);
- from M_c (here $M_c = M_{\pi\pi}$) dependence and its influence on t-dependence we can make some conclusions about the interaction at different space-time scales and interrelation between them. Also we can extract couplings of reggeons to different resonances.

Process $p + p \rightarrow p + \pi + \pi + p$ is the first “standard candle”, which we can use to estimate other CEDP processes. In this section we consider the experimental data on the process and make an attempt to extract the information on couplings of different resonances to Pomeron.

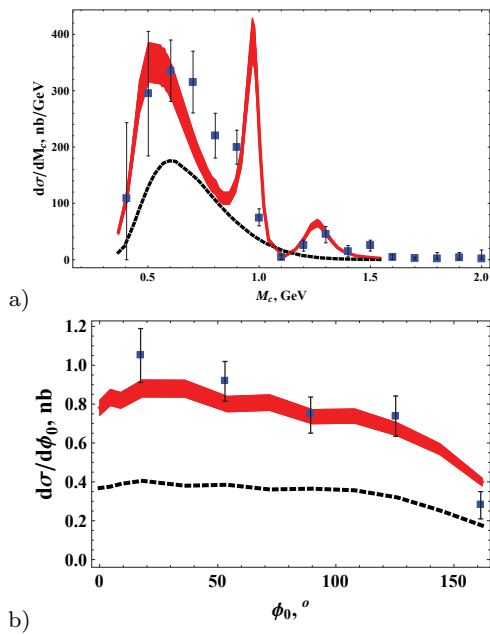


Fig. 5 The data on the process $p + p \rightarrow p + \pi^+ + \pi^- + p$ at $\sqrt{s} = 200$ GeV (STAR collaboration [21],[22]): (a) $|\eta_\pi| < 1$, $|\eta_{\pi\pi}| < 2$, $p_{T\pi} > 0.15$ GeV, $0.005 < -t_{1,2} < 0.03$ GeV²; (b) plus additional cut $M_c < 1$ GeV. Curves correspond to $\Lambda_\pi = 1.2$ GeV in the off-shell pion form factor (9) and couplings from (12). Solid upper curves correspond to the sum of all amplitudes and dashed lower ones represent the continuum contribution. Thickness of the solid curves corresponds to the errors of Monte-Carlo calculations.

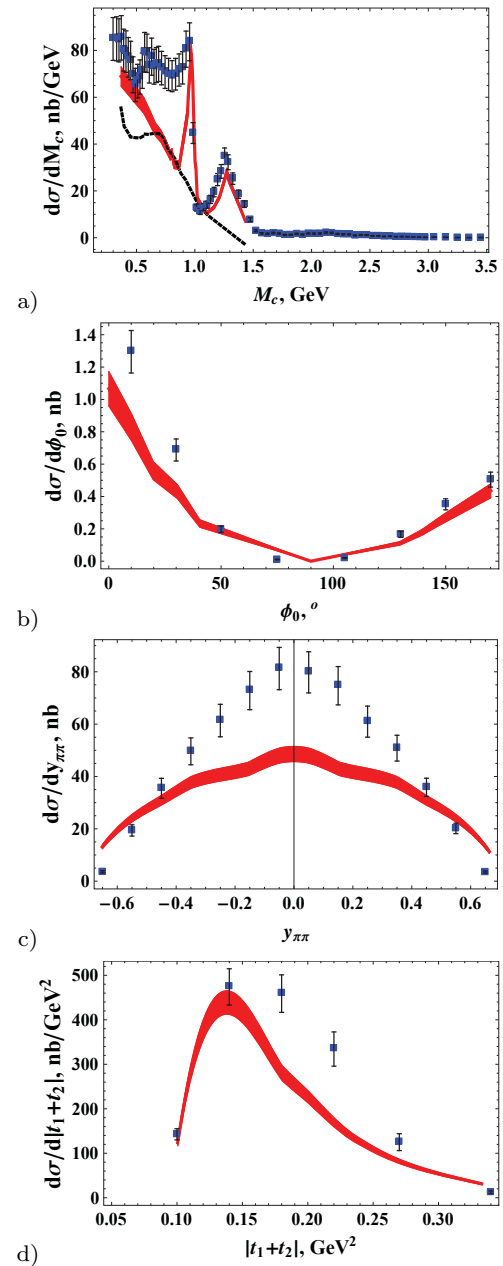


Fig. 6 The new data on the process $p + p \rightarrow p + \pi^+ + \pi^- + p$ at $\sqrt{s} = 200$ GeV (STAR collaboration [23]-[25]): $|\eta_\pi| < 0.7$, $p_{T\pi} > 0.2$ GeV, $p_x > -0.2$ GeV, 0.2 GeV $< |p_y| < 0.4$ GeV, $(p_x + 0.3 \text{ GeV})^2 + p_y^2 < 0.25$ GeV², where p denotes the momenta of final protons. Curves correspond to $\Lambda_\pi = 1.2$ GeV in the off-shell pion form factor (9) and couplings from (12). Solid curves correspond to the sum of all amplitudes and the dashed lower one in (a) represents the continuum contribution. Thickness of the solid curves corresponds to the errors of Monte-Carlo calculations.

2.1 STAR collaboration data versus model cases

In this subsection the data of the STAR collaboration [21]-[26] and model curves for continuum and the

sum of all cases of Fig. 1 are presented. In our approach we have several free parameters: A_π (for the continuum) and couplings of resonances to Pomeron $g_{\mathbb{P}P_f}$, which we can extract from the data. All the distributions are depicted here for $A_\pi = 1.2$ GeV and couplings from (12).

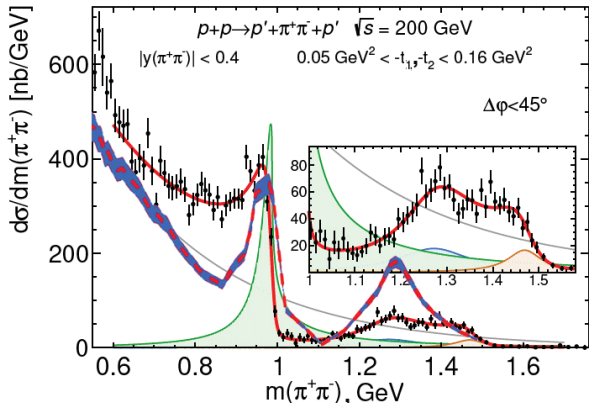


Fig. 7 The new data on the process $p + p \rightarrow p + \pi^+ + \pi^- + p$ at $\sqrt{s} = 200$ GeV (STAR collaboration [23]-[25]): $|y_{\pi\pi}| < 0.4$, $0.05 \text{ GeV}^2 < |t_{1,2}| < 0.16 \text{ GeV}^2$, $\phi_0 < 45^\circ$. Dashed curve corresponds to parameters, fixed from the old data from STAR depicted in the Fig. 5 and explained in the text: $A_\pi = 1.2$ GeV in the off-shell pion form factor (9) and couplings from (12).

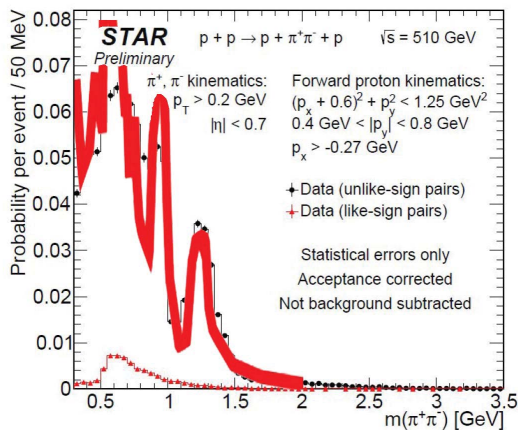


Fig. 8 The new preliminary data on the process $p + p \rightarrow p + \pi^+ + \pi^- + p$ at $\sqrt{s} = 510$ GeV (STAR collaboration [26]): $|\eta_\pi| < 0.7$, $p_{T\pi} > 0.2$ GeV, $p_x > -0.27$ GeV, $0.4 \text{ GeV} < |p_y| < 0.8 \text{ GeV}$, $(p_x + 0.6 \text{ GeV})^2 + p_y^2 < 1.25 \text{ GeV}^2$, where p denotes the momenta of final protons. Theoretical solid curve correspond to $A_\pi = 1.2$ GeV in the off-shell pion form factor (9) and couplings from (12). Fluctuations are due to complex Monte-Carlo integration process, and they can be smoothed by increasing the integration accuracy.

We begin our analysis by fitting the data from STAR depicted on the Fig. 5(a). Then we make predictions for other available data on this process.

First of all we have to note a difference between the data and prediction at the same energy. In the Fig. 5(b) one can see the azimuthal angle distribution. Here we could explain some difference, because our Pomeron-Pomeron-meson couplings are constants, but in reality they depends on the azimuthal angle. The next case, which is depicted in Figs. 6 is more interesting. We see that predictions underestimate the data in the region of $M_c \sim 0.8 \pm 0.1$ GeV as in the Fig. 5(a). The data are close to predictions in the regions of f mesons. This fact can not be understood at the moment, since, if we fix parameters using this new STAR data from Figs. 6, we will obtain overestimation of the data at higher energies, which looks strange. Maybe we have to renormalize this part of the STAR data, or Pomeron-Pomeron-meson couplings have some complex dependence on $t_{1,2}$ and ϕ_0 . It should be checked in further investigations. The ρ contribution is small. We also see some differences in Figs. 6(b,c,d).

The data for extended kinematical region at $\sqrt{s} = 200$ GeV is depicted in the Fig. 7 with the theoretical curve, which is slightly underestimate the data at low masses and overestimate the data at the peak of $f_2(1270)$. Since these data were obtained by some extrapolation, it can be considered only qualitatively.

In the Fig. 8 we see the similar situation with overestimation at $M_c \sim 0.7 \pm 0.2$ GeV and at the peak of $f_0(980)$.

2.2 ISR and CDF data versus the model curves

Let us look at the ISR [19],[20] and CDF [27],[28] data with parameter A_π , which we use to describe the data from STAR collaboration. Different cases are depicted on Figs. 9-10.

We see strong underestimation of the ISR data (by factor of 3). For these low energies we have to take into account possible corrections to pion-proton amplitudes (contributions from secondary reggeons are strong), since our approach describe data well only for energies greater than ~ 3 GeV. And in each shoulder ($T_{\pi p}$ amplitude in Fig. 1 (a),(b)) energy can be less than 3 GeV. Also contributions from single and double dissociations are possible.

As to the CDF data in the Fig. 10(a), it is close to the predictions at the region of $f_2(1270)$ meson. And another part of the CDF data in the Fig. 10(b) is close to the prediction, but the curve does not fit the data at the region of $f_2(1270)$ meson. It also looks strange

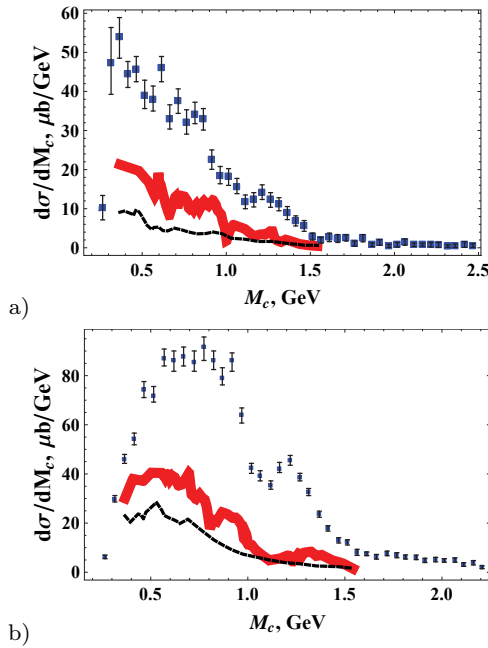


Fig. 9 The data on the process $p+p \rightarrow p+\pi^++\pi^-+p$ (ISR and ABCDHW collaborations [19],[20]): (a) at $\sqrt{s} = 63$ GeV, $|y_\pi| < 1$, $\xi_p > 0.9$; (b) at $\sqrt{s} = 62$ GeV, $|y_\pi| < 1.5$, $\xi_p > 0.9$. Curves correspond to $\Lambda_\pi = 1.2$ GeV in the off-shell pion form factor (9) and couplings from (12). Solid upper curves correspond to the sum of all amplitudes and dashed lower ones represent the continuum contribution. Fluctuations in solid curves are due to complex Monte-Carlo integration process, and they can be smoothed by increasing the integration accuracy. Thickness of the solid curves corresponds to the errors of Monte-Carlo calculations.

and has no explanation at the moment, since this is the data from the same experiment. This is may be due to interference effects with $\gamma\gamma$ or $\gamma\mathbb{O}$ fusion in the central production process and corrections to $\pi\pi$ final interaction.

2.3 CMS data and predictions

In Fig. 11 one can see the recent data from the CMS collaboration and curves of our model, which correspond to $\Lambda_\pi = 1.2$ GeV in the off-shell pion form factor (9) and couplings (12) from the fit to the STAR data on Fig. 6. Here our predictions are very close to the data except for the region $M_c \sim 0.8 \pm 0.1$ GeV, as in all datasets.

Summary and conclusions

In this paper we have considered the process LM CEDP of di-pions and its description in the framework of the

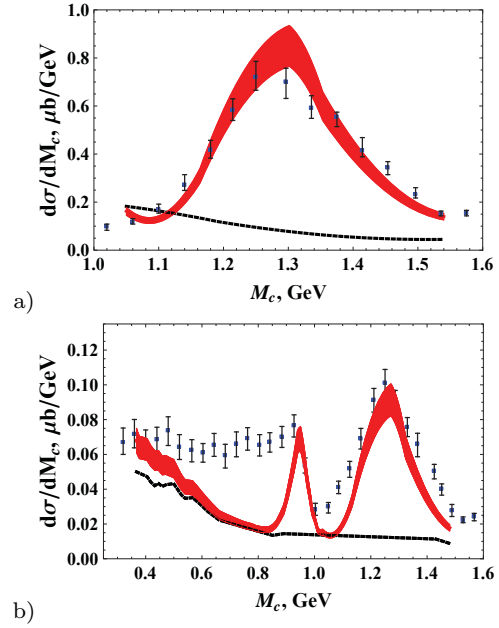


Fig. 10 The data on the process $p+\bar{p} \rightarrow p+\pi^++\pi^-+\bar{p}$ (CDF collaboration [27],[28]) at $\sqrt{s} = 1.96$ TeV: (a) $|\eta_\pi| < 1.3$, $|y_{\pi\pi}| < 1$, $p_{T,\pi} > 0.4$ GeV; (b) $|\eta_\pi| < 1.3$, $|y_{\pi\pi}| < 1$, $p_{T,\pi} > 0.4$ GeV, $p_{T,\pi\pi} > 1$ GeV. Curves correspond to $\Lambda_\pi = 1.2$ GeV in the off-shell pion form factor (9) and couplings from (12). Solid upper curves correspond to the sum of all amplitudes and dashed lower ones represent the continuum contribution. Fluctuations in solid curves are due to complex Monte-Carlo integration process, and they can be smoothed by increasing the integration accuracy. Thickness of the solid curves corresponds to the errors of Monte-Carlo calculations.

Regge-eikonal approach. Here we summarize all the facts and conclusions:

- The result is crucially dependent on the choice of Λ_π in the off-shell pion form factor, i.e. on \hat{t} (virtuality of the pion) dependence. In the present approach the best description of the old STAR data [21],[22] is given by the case with $\Lambda_\pi = 1.2$ GeV and couplings:

$$\begin{aligned} g_{\text{PP}f_0(500)} &= 0.88, \\ g_{\text{PP}f_0(980)} &= 0.43, \\ g_{\text{PP}f_2(1270)} &= 1.72. \end{aligned} \quad (12)$$

The couplings of Pomeron to $f_{0,2}$ can be compared to the value 0.64, which is obtained in [39].

- the model shows that contributions from ρ meson are not so significant at available energies, but we have a dip in the theoretical curves at the region of ρ production (at CMS energies, for example, it is obvious). This also should be explained in further investigations.
- Rescattering corrections (“soft survival probability”) in pp and πp make a significant contribution to the values and form of distributions.

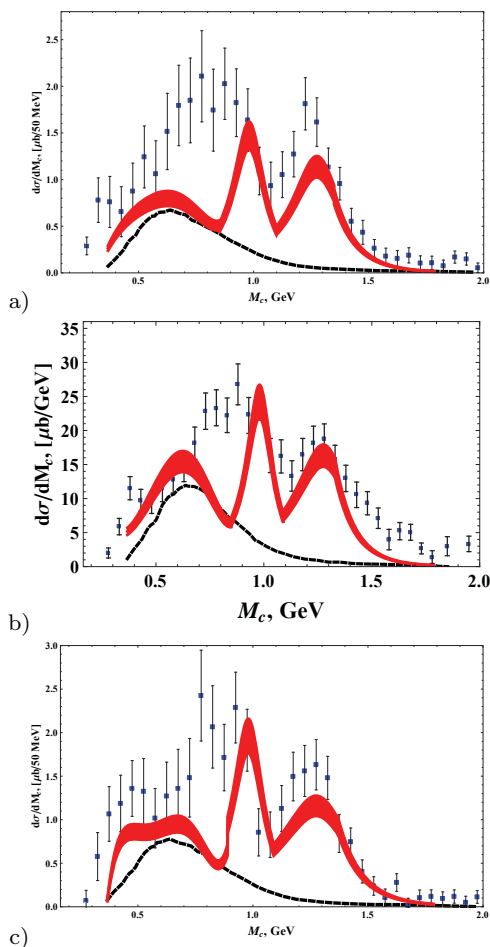


Fig. 11 The data on the process $p + p \rightarrow p + \pi^+ + \pi^- + p$ (CMS collaboration [29],[30]): (a) at $\sqrt{s} = 5$ TeV with cuts $|\eta_\pi| < 2.4$, $p_{T,\pi} > 0.2$ GeV; (b) at $\sqrt{s} = 7$ TeV with cuts $|\eta_\pi| < 2$, $p_{T,\pi} > 0.2$ GeV; (c) at $\sqrt{s} = 13$ TeV with cuts $|\eta_\pi| < 2.4$, $p_{T,\pi} > 0.2$ GeV. Curves correspond to $\Lambda_\pi = 1.2$ GeV in the off-shell pion form factor (9) and couplings from (12). Solid upper curves correspond to the sum of all amplitudes and dashed lower ones represent the continuum contribution. Thickness of the solid curves corresponds to the errors of Monte-Carlo calculations.

- If we try to fit the data from STAR [23]-[26], we find that the curves with parameters fixed from [21],[22] underestimate the data in the region of ρ meson as in the Fig.5(a). The data are close to predictions only in the regions of f mesons. These effects have no explanation at the moment, and may be due to some complex dependance of Pomeron-Pomeron-meson couplings on $t_{1,2}$ and ϕ_0 , wrong normalization of the data or missed contributions from some other processes like low mass diffractive dissociation.
- We have strong underestimation of the ISR data (by factor of 3) [19],[20] and contradictory description of two parts of the CDF data [27],[28] with the same parameters (see Figs.9,10).

- However, the CMS data at all energies are described rather well (see Fig. 11). Discrepancy is observed only in the region $M_c \sim 0.8 \pm 0.2$ GeV as for other energies.

The main open problems regarding model parameters are related to interference terms (we have to know all cut-off form-factor parameters, couplings of pions and reggeons to resonances and their dependance on $t_{1,2}$ and ϕ_0). To fix the model parameters correctly we need the comparison with precise (exclusive) experimental data (STAR, ATLAS+ALFA, CMS+TOTEM) simultaneously in several differential observables, e.g. the differential distributions $d\sigma/dt_1$, $d\sigma/d\phi_0$, the angular distributions in the $\pi^+\pi^-$ rest system and others. It should be done in further works.

We have to take into account also effects like the interference with $\gamma\gamma \rightarrow \pi\pi$ and $\gamma\mathbb{O} \rightarrow \pi\pi$ processes, effects related to the irrelevance and possible modifications of the Regge approach (for the virtual pion exchange) in this kinematical region, as was discussed in the introduction, corrections to pion-pion scattering at low $M_{\pi\pi}$, corrections to $T_{\pi p}(s, t)$ for $\sqrt{s} < 3$ GeV, difference of resonance peaks from the Breit-Wigner functions. In further works we will take into account possible modifications of the model for best description of the data.

This model will be implemented to the Monte-carlo event generator ExDiff [40]. It is possible to calculate LM CEDP for other di-hadron final states ($p\bar{p}$ for “Odderon” hunting, K^+K^- , $\eta\eta'$ and so on), which are also very informative for our understanding of diffractive mechanisms in strong interactions.

Acknowledgements

I am grateful to Vladimir Petrov, Anton Godizov and Piotr Lebedowicz for useful discussions and help.

Appendix A. Kinematics of LM CEDP

The $2 \rightarrow 4$ process $p(p_a) + p(p_b) \rightarrow p(p_1) + \pi(p_3) + \pi(p_4) + p(p_2)$ can be described as follows (the notation

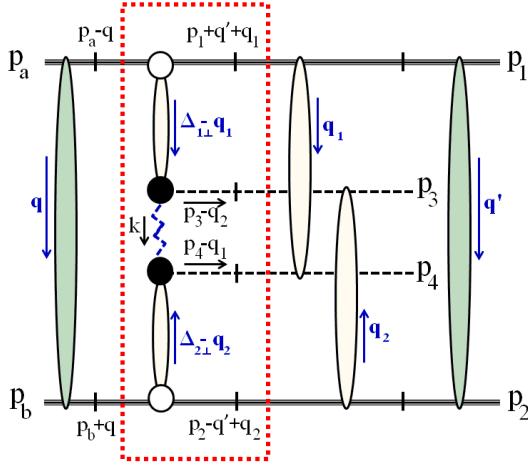


Fig. 12 Total amplitude of the process of double pion LM CEDP $p + p \rightarrow p + \pi^+ + \pi^- + p$ with detailed kinematics. Proton-proton rescatterings in the initial and final states are depicted as black blobs, and pion-proton subamplitudes are also shown as shaded blobs. All momenta are shown. Basic part of the amplitude, M_0 (see eq. (3)), without corrections is circled by a dotted line. Crossed lines are on mass shell. Here $\Delta_{1\perp} = \Delta_1 - q - q'$, $\Delta_{2\perp} = \Delta_2 + q + q'$, $\hat{t} = k^2 = (\Delta_{1\perp} - q_1 - p_3 + q_2)^2$, $\hat{u} = (\Delta_{1\perp} - q_1 - p_4)^2$, $\hat{s} = (p_3 + p_4 - q_1 - q_2)^2$.

for any momentum is $k = (k_0, k_z; \vec{k})$, $\vec{k} = (k_x, k_y)$:

$$p_a = \left(\frac{\sqrt{s}}{2}, \beta \frac{\sqrt{s}}{2}; \vec{0} \right), p_b = \left(\frac{\sqrt{s}}{2}, -\beta \frac{\sqrt{s}}{2}; \vec{0} \right),$$

$$p_{1,2} = (E_{1,2}, p_{1,2z}; \vec{p}_{1,2\perp}), E_{1,2} = \sqrt{p_{1,2z}^2 + \vec{p}_{1,2\perp}^2 + m_p^2},$$

$$p_{3,4} = (m_{3,4\perp} \text{ch } \eta_{3,4}, m_{3,4\perp} \text{sh } \eta_{3,4}; \vec{p}_{3,4\perp}) =$$

$$= \left(\sqrt{m_\pi^2 + \vec{p}_{3,4\perp}^2} \text{ch } \eta_{3,4}, |\vec{p}_{3,4\perp}| \text{sh } \eta_{3,4}; \vec{p}_{3,4\perp} \right),$$

$$m_{i\perp}^2 = m_i^2 + \vec{p}_{i\perp}^2, m_{1,2} = m_p, m_{3,4} = m_\pi,$$

$$\vec{p}_{4\perp} = -\vec{p}_{3\perp} - \vec{p}_{1\perp} - \vec{p}_{2\perp},$$

$$\beta = \sqrt{1 - \frac{4m_p^2}{s}}, s = (p_a + p_b)^2, s' = (p_1 + p_2)^2. \quad (13)$$

Here y_i (η_i) are rapidities (pseudorapidities) of final pions.

Phase space of the process in terms of the above variables is the following

$$d\Phi_{2 \rightarrow 4} = (2\pi)^4 \delta^4 \left(p_a + p_b - \sum_{i=1}^4 p_i \right) \prod_{i=1}^4 \frac{d^3 p_i}{(2\pi)^3 2E_i} =$$

$$= \frac{1}{2^4 (2\pi)^8} \prod_{i=1}^3 p_{i\perp} dp_{i\perp} d\phi_i \cdot dy_3 dy_4 \cdot \mathcal{J};$$

$$\mathcal{J} = \frac{dp_{1z}}{E_1} \frac{dp_{2z}}{E_2} \delta \left(\sqrt{s} - \sum_{i=1}^4 E_i \right) \delta \left(\sum_{i=1}^4 p_{iz} \right) =$$

$$= \frac{1}{|\vec{E}_2 \tilde{p}_{1z} - \vec{E}_1 \tilde{p}_{2z}|}, \quad (14)$$

where $p_{i\perp} = |\vec{p}_i|$, $\tilde{p}_{1,2z}$ are appropriate roots of the system

$$\begin{cases} A = \sqrt{s} - E_3 - E_4 = \sqrt{m_{1\perp}^2 + p_{1z}^2} + \sqrt{m_{2\perp}^2 + p_{2z}^2}, \\ B = -p_{3z} - p_{4z} = p_{1z} + p_{2z}, \end{cases} \quad (15)$$

$$\tilde{p}_{1z} = \frac{B}{2} + \frac{1}{2(A^2 - B^2)} \left[B(m_{1\perp}^2 - m_{2\perp}^2) + A \cdot \lambda_0^{1/2} \right],$$

$$\lambda_0 = \lambda(A^2 - B^2, m_{1\perp}^2, m_{2\perp}^2). \quad (16)$$

Here $\lambda(x, y, z) = x^2 + y^2 + z^2 - 2xy - 2xz - 2yz$, and then $\mathcal{J}^{-1} = \lambda_0^{1/2}/2$.

For the differential cross-section we have

$$\frac{d\sigma_{2 \rightarrow 4}}{\prod_{i=1}^3 dp_{i\perp} d\phi_i \cdot dy_3 dy_4} = \frac{1}{2\beta s} \cdot \frac{\prod_{i=1}^3 p_{i\perp}}{2^4 (2\pi)^8 \cdot \frac{1}{2} \lambda_0^{1/2}} |T|^2 =$$

$$= \frac{\prod_{i=1}^3 p_{i\perp}}{2^{12} \pi^8 \beta s \lambda_0^{1/2}} |T|^2. \quad (17)$$

Pseudorapidity is more convenient experimental variable, and we can use the transform

$$\frac{dy_i}{d\eta_i} = \frac{p_{i\perp} \text{ch } \eta_i}{\sqrt{m_i^2 + p_{i\perp}^2} \text{ch}^2 \eta_i} \quad (18)$$

to get the differential cross-section in pseudorapidities.

In some cases it is convenient to use other variables for the integration of the cross-section and calculation of distributions on central mass. For these cases we have:

$$d\Phi_{2 \rightarrow 4} = \frac{1}{2^4 (2\pi)^8} \prod_{i=1}^2 dt_i d\phi_i \cdot M_c dM_c d\eta_c dc^* d\phi^* \cdot \mathcal{J}';$$

$$\mathcal{J}' = \frac{\beta_M}{4\beta_1 \beta_2 s} \frac{dy_c}{d\eta_c}, \quad \beta_i \simeq \sqrt{1 + \frac{4(m_p^2 - (1 - \xi_i)t_i)}{\beta^2 s^2 (1 - \xi_i)^2}};$$

$$\beta_M = \sqrt{1 - \frac{4m_\pi^2}{M_c^2}}, \quad \frac{dy_c}{d\eta_c} = \frac{p_{c\perp} \text{ch } \eta_c}{\sqrt{M_c^2 + p_{c\perp}^2} \text{ch}^2 \eta_c}; \quad (19)$$

$$\frac{d\sigma_{2 \rightarrow 4}}{\prod_{i=1}^2 dt_i d\phi_i dM_c d\eta_c dc^* d\phi^*} = \frac{1}{2\beta s} \cdot \frac{M_c \beta_M \frac{dy_c}{d\eta_c}}{2^4 (2\pi)^8 \cdot 4\beta_1 \beta_2 s} |T|^2 =$$

$$= \frac{M_c \beta_M \frac{dy_c}{d\eta_c}}{2^{15} \pi^8 \beta_1 \beta_2 s^2} |T|^2, \quad (20)$$

where $c^* = \cos \theta^*$, θ^* and ϕ^* are polar and azimuthal angles of the pion momenta in the $\pi^+ \pi^-$ rest frame, M_c is the di-pion mass, η_c is the di-pion pseudorapidity, $t_1 = (p_a - p_1)^2$, $t_2 = (p_b - p_2)^2$ and

$$\xi_{1,2} \simeq \sqrt{\frac{M_c^2 - t_1 - t_2 + 2\sqrt{t_1 t_2} \cos(\phi_1 - \phi_2)}{s}} \mathbf{e}_{\pm y_c}.$$

For exact calculations of elastic subprocesses (see Fig. 12) of the type

$$a(p_1) + b(p_2) \rightarrow c(p_1 - q_{el}) + d(p_2 + q_{el}):$$

$$\begin{aligned} q_{el} &= (q_0, q_z; \vec{q}), \\ q_z &= -\frac{b}{2a} \left(1 - \sqrt{1 - \frac{4ac}{b^2}} \right), \\ q_0 &= \frac{A_0 q_z + \vec{p}_{1\perp} \vec{q} + \vec{p}_{2\perp} \vec{q}}{A_z}, \\ a &= A_z^2 - A_0^2, \quad b = -2(A_z \cdot \mathcal{D} + A_0(\vec{p}_{1\perp} \vec{q} + \vec{p}_{2\perp} \vec{q})), \\ c &= 2A_z B_z - (\vec{p}_{1\perp} \vec{q} + \vec{p}_{2\perp} \vec{q})^2 + \vec{q}^2 A_z^2, \\ A_0 &= p_{1z} + p_{2z}, \quad A_z = p_{10} + p_{20}, \\ B_0 &= p_{1z} \cdot \vec{p}_{2\perp} \vec{q} - p_{2z} \cdot \vec{p}_{1\perp} \vec{q}, \\ B_z &= p_{10} \cdot \vec{p}_{2\perp} \vec{q} - p_{20} \cdot \vec{p}_{1\perp} \vec{q}, \\ \mathcal{D} &= p_{1z} p_{20} - p_{2z} p_{10}, \end{aligned} \quad (21)$$

and $q_{el}^2 \simeq -\vec{q}^2$.

Appendix B. Regge-eikonal model for elastic proton-proton and pion-proton scattering

Here is a short review of formulae for the Regge-eikonal approach [32], [33], which we use to estimate rescattering corrections in the proton proton and pion proton channels.

Amplitudes of elastic proton-proton and pion-proton scattering are expressed in terms of eikonal functions

$$\begin{aligned} T_{pp,\pi p}^{el}(s, b) &= \frac{e^{-2\Omega_{pp,\pi p}^{el}(s, b)} - 1}{2i}, \\ \Omega_{pp,\pi p}^{el}(s, b) &= -i\delta_{pp,\pi p}^{el}(s, b), \\ \delta_{pp,\pi p}^{el}(s, b) &= \frac{1}{16\pi s} \int_0^\infty d(-t) J_0(b\sqrt{-t}) \delta_{pp,\pi p}^{el}(s, t). \end{aligned} \quad (22)$$

$$\begin{aligned} \delta_{pp}^{el}(s, t) &\simeq \\ g_{pp\mathbb{P}}(t)^2 \left(i + \tan \frac{\pi(\alpha_{\mathbb{P}}(t) - 1)}{2} \right) \pi \alpha'_{\mathbb{P}}(t) \left(\frac{s}{2s_0} \right)^{\alpha_{\mathbb{P}}(t)}, \\ \alpha_{\mathbb{P}}(t) &= 1 + \frac{\alpha_{\mathbb{P}}(0) - 1}{1 - \frac{t}{\tau_a}}, \quad g_{pp\mathbb{P}}(t) = \frac{g_{pp\mathbb{P}}(0)}{(1 - a_g t)^2}. \end{aligned} \quad (23)$$

$$\begin{aligned} \delta_{\pi p}^{el}(s, t) &\simeq \\ \left(i + \tan \frac{\pi(\alpha_{\mathbb{P}}(t) - 1)}{2} \right) \beta_{\mathbb{P}}(t) \left(\frac{s}{s_0} \right)^{\alpha_{\mathbb{P}}(t)}, \\ + \left(i + \tan \frac{\pi(\alpha_f(t) - 1)}{2} \right) \beta_f(t) \left(\frac{s}{s_0} \right)^{\alpha_f(t)}, \end{aligned} \quad (24)$$

$$\begin{aligned} \alpha_{\mathbb{P}}(t) &= 1 + p_1 \left[1 - p_2 t \left(\arctan(p_3 - p_2 t) - \frac{\pi}{2} \right) \right], \\ \alpha_f(t) &= \left(\frac{8}{3\pi} \gamma(\sqrt{-t + c_f}) \right)^{1/2}, \\ \gamma(\mu) &= \frac{4\pi}{11 - \frac{2}{3}n_f} \left(\frac{1}{\ln \frac{\mu^2}{\Lambda^2}} + \frac{1}{1 - \frac{\mu^2}{\Lambda^2}} \right), \\ \beta_{\mathbb{P}}(t) &= B_{\mathbb{P}} e^{b_{\mathbb{P}} t} (1 + d_1 t + d_2 t^2 + d_3 t^3 + d_4 t^4), \\ \beta_f(t) &= B_f e^{b_f t}. \end{aligned} \quad (25)$$

Parameters can be found in tables 1 and 2.

Table 1 Parameters for proton-proton elastic scattering amplitude.

Parameter	Value
$\alpha_{\mathbb{P}}(0) - 1$	0.109
τ_a	0.535 GeV ²
$g_{pp\mathbb{P}}(0)$	13.8 GeV
a_g	0.23 GeV ⁻²

Table 2 Parameters for pion-proton elastic scattering amplitude.

Parameter	Value
$B_{\mathbb{P}}$	26.7
$b_{\mathbb{P}}$	2.36 GeV ⁻²
d_1	0.38 GeV ⁻²
d_2	0.3 GeV ⁻⁴
d_3	-0.078 GeV ⁻⁶
d_4	0.04 GeV ⁻⁸
B_f	67
b_f	1.88 GeV ⁻²

$$\begin{aligned}
V_{pp}(s, q^2) &= \int d^2\vec{b} e^{i\vec{q}\vec{b}} \sqrt{1 + 2iT_{pp}^{el}(s, b)} = \\
&= \int d^2\vec{b} e^{i\vec{q}\vec{b}} e^{-\Omega_{pp}^{el}(s, b)} = \\
&= (2\pi)^2 \delta^2(\vec{q}) + 2\pi \bar{T}_{pp}(s, q^2), \quad (26)
\end{aligned}$$

$$\bar{T}_{pp}(s, q^2) = \int_0^\infty b db J_0(b\sqrt{-q^2}) \left[e^{-\Omega_{pp}^{el}(s, b)} - 1 \right] \quad (27)$$

$$\begin{aligned}
S_{\pi p}(s, q^2) &= \int d^2\vec{b} e^{i\vec{q}\vec{b}} (1 + 2iT_{\pi p}^{el}(s, b)) = \\
&= \int d^2\vec{b} e^{i\vec{q}\vec{b}} e^{-2\Omega_{\pi p}^{el}(s, b)} = \\
&= (2\pi)^2 \delta^2(\vec{q}) + 2\pi \bar{T}_{\pi p}(s, q^2), \quad (28)
\end{aligned}$$

$$\bar{T}_{\pi p}(s, q^2) = \int_0^\infty b db J_0(b\sqrt{-q^2}) \left[e^{-2\Omega_{\pi p}^{el}(s, b)} - 1 \right] \quad (29)$$

Here we take $S_{\pi p}(s, t) = S_{\pi+p}(s, t) = S_{\pi-p}(s, t)$ and

$$T_{\pi+p}^{el}(s, t) = T_{\pi-p}^{el}(s, t) = 4\pi s \bar{T}_{\pi p}(s, t) \quad (30)$$

Approach (24) describes the data on pion-proton scattering better even at low energies, that is why we use it instead of the one presented in [32].

Functions \bar{T}_{pp} and $\bar{T}_{\pi p}$ are convenient for numerical calculations, since its oscillations are not so strong.

Appendix C. Primary amplitudes for CEDP and ERVM resonance production.

Here is the short review of the formulae, which can be obtained by the use of Refs. [34], [39] and [14]-[17].

Let us introduce the general diffractive factor

$$F_{\mathbb{P}}(t, \xi) = g_{pp\mathbb{P}}(t)^2 \left(i + \tan \frac{\pi(\alpha_{\mathbb{P}}(t) - 1)}{2} \right) \frac{\pi \alpha'_{\mathbb{P}}(t)}{\xi^{\alpha_{\mathbb{P}}(t)}}. \quad (31)$$

f_0 production

For f_0 production we have the following expression

$$\begin{aligned}
M_0^{pp \rightarrow p\{f_0 \rightarrow \pi^+ \pi^-\}p} &= \\
&= -F_{\mathbb{P}}(t_1, \xi_1) F_{\mathbb{P}}(t_2, \xi_2) g_{\mathbb{P}f_0}(t_1, t_2, M_c^2) \times \\
&\times \frac{g_{f_0\pi\pi} \left(\mathcal{F}(M_c^2, m_{f_0}^2) \right)^2 F_M(t_1) F_M(t_2)}{(M_c^2 - m_{f_0}^2) + B_{f_0}(M_c^2, m_{f_0}^2)}, \quad (32)
\end{aligned}$$

where ($M_c > 2m_\pi$)

$$\begin{aligned}
B_{f_0}(M_c^2, m_{f_0}^2) &= \\
&= i \Gamma_{f_0} \left(\mathcal{F}(M_c^2) \right)^2 \left[\frac{1 - 4m_\pi^2/M_c^2}{1 - 4m_\pi^2/m_{f_0}^2} \right]^{1/2} \quad (33)
\end{aligned}$$

$$\begin{aligned}
\mathcal{F}(M_c^2, m_f^2) &= F^{\mathbb{P}\mathbb{P}f}(M_c^2, m_f^2) = F^{f\pi\pi}(M_c^2, m_f^2) = \\
&= \exp \left(\frac{-(M_c^2 - m_f^2)^2}{\Lambda_f^4} \right), \quad \Lambda_f \sim 1 \text{ GeV}, \quad (34)
\end{aligned}$$

$$F_M(t) = 1/(1 - t/m_0^2), \quad m_0^2 = 0.5 \text{ GeV}^2 \quad (35)$$

$\mathcal{F}(M_c^2, m_f^2)$ and $F_M(t)$ are off-shell phenomenological form-factors introduced in [14]-[17] to make more good description of the data. Here we fix mass and width of $f_0(500)$ and $f_0(980)$ mesons as in [15]

$$m_{f_0(500)} = 0.6 \text{ GeV}, \quad \Gamma_{f_0(500)} = 0.5 \text{ GeV}, \quad (36)$$

$$m_{f_0(980)} = 0.98 \text{ GeV}, \quad \Gamma_{f_0(980)} = 0.07 \text{ GeV}, \quad (37)$$

and also their couplings to pions

$$g_{f_0(500)\pi\pi} = 3.37, \quad g_{f_0(980)\pi\pi} = 1.55, \quad (38)$$

assuming also $\Gamma(f_0 \rightarrow \pi\pi)/\Gamma_{f_0} = 100\%$.

In this work coupling of Pomeron to meson $g_{\mathbb{P}f_0}$ is the constant and can be extracted from the experimental data as a free parameter. In [39] this coupling is proposed to be 0.64 GeV for all mesons related to the ‘‘glueball state’’. Here due to simplifications these couplings are of the same order, but may differ by factor $2 \div 3$ (see the main text).

f_2 production

For $f_2(1270)$ production we have to modify the expression (32) due to the tensor nature of this meson. Finally we have

$$\begin{aligned}
M_0^{pp \rightarrow p\{f_2 \rightarrow \pi^+ \pi^-\}p} &= \\
&= F_{\mathbb{P}}(t_1, \xi_1) F_{\mathbb{P}}(t_2, \xi_2) g_{\mathbb{P}f_2} \times \\
&\times \frac{(g_{f_2\pi\pi}/2) \left(\mathcal{F}(M_c^2, m_{f_2}^2) \right)^2 F_M(t_1) F_M(t_2)}{(M_c^2 - m_{f_2}^2) + B_{f_2}(M_c^2, m_{f_2}^2)} \mathcal{P}_2, \quad (39)
\end{aligned}$$

where

$$\mathcal{P}_2 = (\Delta_1 \Delta_{34})^2 - \frac{(M_c^2 - 4m_\pi^2) \lambda(M_c^2, t_1, t_2)}{12M_c^2} \quad (40)$$

is the additional function which can be obtained by contraction of Pomeron-Pomeron-meson vertex with pion-pion-meson one, $\Delta_1 = p_a - p_1$, $\Delta_{34} = p_3 - p_4$.

$$\begin{aligned}
B_{f_2}(M_c^2, m_{f_2}^2) &= \\
&= i \Gamma_{f_2} \left(\mathcal{F}(M_c^2, m_{f_2}^2) \right)^2 \left[\frac{1 - 4m_\pi^2/M_c^2}{1 - 4m_\pi^2/m_{f_2}^2} \right]^{5/2} \frac{M_c^4}{m_{f_2}^4} \quad (41)
\end{aligned}$$

Fixed parameters for $f_2(1270)$ are

$$\begin{aligned} m_{f_2(1270)} &= 1.275 \text{ GeV}, \quad \Gamma_{f_2(1270)} = 0.1851 \text{ GeV}, \\ g_{f_2(1270)\pi\pi} &= 9.26 \text{ GeV}^{-1}, \quad \Lambda_{f_2} = 1 \text{ GeV}. \end{aligned} \quad (42)$$

After the data analysis the ‘‘scalar’’ coupling of the $f_2(1270)$ to Pomeron is found to be of the order of 2. Since the Pomeron does not behave as a simple scalar, the structure of the coupling is, of course, more complicated. In the ‘‘exact’’ model like in [14] Pomeron can be a coherent sum of different spins, and have several couplings to f mesons. But in real life we have to obtain the vertex for any spin J and then to make a continuation to the complex plane in J , like in classical Regge theory. This is the conceptual question, which was partially discussed in [3], but we postpone it to our further theoretical works. And in the present work we use simplified model for the f_2 production. That is why the extracted value of the ‘‘constant’’ coupling could differ from the real set of tensor couplings.

ρ_0 production

For ρ_0 situation is a little bit complicated, since we have to take into account vector dominance and also $\rho - \omega$ mixing. After all contractions the primary amplitude looks as follows

$$\begin{aligned} M_0^{pp \rightarrow p\{\rho_0 \rightarrow \pi^+\pi^-\}p} &= i T_{\rho_0 p}^{el}(s_2, t_2) \frac{C_T^{\rho_0}(t_1) \mathcal{P}_\rho}{|t_1|} \times \\ &\times \frac{(g_{\rho_0 \pi \pi}/2) \mathcal{F}_\rho(M_c^2) \mathcal{F}_\rho(t_1)}{(M_c^2 - m_{\rho_0}^2) + B_{\rho_0}(M_c^2, m_{\rho_0}^2)} + (1 \leftrightarrow 2), \end{aligned} \quad (43)$$

$$s_2 = (p_3 + p_4 + p_2)^2 = (p_a - p_1 + p_b)^2,$$

$$s_1 = (p_3 + p_4 + p_1)^2 = (p_b - p_2 + p_a)^2.$$

Amplitude $T_{\rho_0 p}^{el}(s, t)$ can be obtained by the use of the formulae similar to (22)-(24) with

$$\begin{aligned} \delta_{\rho_0 p}^{el}(s, t) &\simeq g_{pp\mathbb{P}}(t) g_{\rho\rho\mathbb{P}}(t) \left(i + \tan \frac{\pi(\alpha_{\mathbb{P}}(t) - 1)}{2} \right) \times \\ &\times \pi \alpha'_{\mathbb{P}}(t) \left(\frac{s}{2s_0} \right)^{\alpha_{\mathbb{P}}(t)}, \\ g_{\rho\rho\mathbb{P}}(t) &= g_{\rho\rho\mathbb{P}}(0) = 7.07 \text{ GeV} \quad (\text{see [34]}); \end{aligned} \quad (44)$$

$$C_T^{\rho_0}(t) = \sqrt{\frac{3\Gamma_{\rho \rightarrow e^+e^-}}{\alpha_e m_\rho}} \frac{m_\rho^2}{m_\rho^2 - t}, \quad (45)$$

$$\mathcal{F}_\rho(p^2) = (1 + p^2(p^2 - m_\rho^2)/\Lambda_\rho^4)^{-n_\rho}, \quad (46)$$

$$F_1(t) = \frac{1 - \kappa t/(4m_\rho^2)}{1 - t/(4m_\rho^2)} (1 - t/m_D^2)^{-2}, \quad (47)$$

$$\kappa = \mu_p/\mu_N = 2.7928, \quad m_D^2 = 0.71 \text{ GeV}^2, \quad (48)$$

$$\Gamma_{\rho \rightarrow e^+e^-} = 7.04 \cdot 10^{-6} \text{ GeV}, \quad (49)$$

$$\mathcal{P}_\rho \simeq 2\sqrt{4\pi\alpha_e} F_1(t) \left(\vec{\Delta}_{34}^* \vec{p}_a^* \right), \quad (50)$$

\mathcal{P}_ρ is the factor that is equal to ‘‘scalar proton-proton-photon vertex’’ contracted with the vector of $\rho\pi\pi$ vertex, and the scalar product of transverse vectors $\left(\vec{\Delta}_{34}^* \vec{p}_a^* \right)$ in the ρ meson rest frame with

$$\Delta_1^* = \{(M_c^2 + t_1 - t_2)/(2M_c), 0, 0, \lambda^{1/2}/(2M_c)\}$$

can be expressed in terms of four vectors in the central mass frame of colliding protons:

$$\begin{aligned} \left(\vec{\Delta}_{34}^* \vec{p}_a^* \right) &= -\Delta_{34} p_a - \Delta_{34,z}^* p_{a,z}^*, \\ \Delta_{34,z}^* &= -\Delta_1 \Delta_{34} \frac{2M_c}{\lambda^{1/2}}, \\ p_{a,z}^* &= \left(\frac{p_a p_c (M_c^2 + t_1 - t_2)}{2M_c^2} - \frac{t_1}{2} \right) \frac{2M_c}{\lambda^{1/2}}, \\ \lambda &\equiv \lambda(M_c^2, t_1, t_2), \quad p_c = p_3 + p_4. \end{aligned} \quad (51)$$

Other functions and parameters are

$$\begin{aligned} B_{\rho_0}(M_c^2, m_{\rho_0}^2) &= \\ &= i \Gamma_{\rho_0} (\mathcal{F}_\rho(M_c^2))^2 \left[\frac{1 - 4m_\pi^2/M_c^2}{1 - 4m_\pi^2/m_{\rho_0}^2} \right]^{3/2} \frac{M_c}{m_{\rho_0}^2} \end{aligned} \quad (52)$$

$$\begin{aligned} m_{\rho_0} &= 0.7737 \text{ GeV}, \quad \Gamma_{\rho_0} = 0.1462 \text{ GeV}, \\ g_{\rho_0 \pi \pi} &= 11.51 \text{ GeV}, \quad \Lambda_\rho = 1 \text{ GeV}, \quad n_\rho = 0.5. \end{aligned} \quad (53)$$

Here we take for all off-shell propagators of resonances simple Breit-Wigner form, but we can use more complicated expressions, which can be found, for example, in [14]-[17].

$$\begin{aligned} M^U(\{p\}) &= \\ &= \int \int \frac{d^2 \vec{q}}{(2\pi)^2} \frac{d^2 \vec{q}'}{(2\pi)^2} \frac{d^2 \vec{q}_1}{(2\pi)^2} \frac{d^2 \vec{q}_2}{(2\pi)^2} V_{pp}(s, q^2) V_{pp}(s', q'^2) \\ &\times [[S_{\tilde{h}p}(\tilde{s}_{14}, q_1^2) M_0^C(\{\tilde{p}\}) S_{hp}(\tilde{s}_{23}, q_2^2) + (3 \leftrightarrow 4)] + M_0^R(\{\tilde{p}\})] \\ &\approx \int \int \frac{d^2 \vec{q}}{(2\pi)^2} \frac{d^2 \vec{q}_1}{(2\pi)^2} \frac{d^2 \vec{q}_2}{(2\pi)^2} S_{pp}(s, q^2) \\ &\times [[S_{\tilde{h}p}(\tilde{s}_{14}, q_1^2) M_0^C(\{\tilde{p}\}) S_{hp}(\tilde{s}_{23}, q_2^2) + (3 \leftrightarrow 4)] + M_0^R(\{\tilde{p}\})]_{q' \rightarrow 0} \\ M_0^C(\{p\}) &= T_{hp}^{el}(s_{13}, t_1) \mathcal{P}_h(\hat{s}, \hat{t}) \left[\hat{F}_h(\hat{t}) \right]^2 T_{hp}^{el}(s_{24}, t_2), \end{aligned}$$

where functions are defined in (26)-(30) of Appendix B, and sets of vectors are

$$\begin{aligned} \{p\} &\equiv \{p_a, p_b, p_1, p_2, p_3, p_4\} \\ \{\tilde{p}\} &\equiv \{p_a - q, p_b + q; p_1 + q' + q_1, \\ &\quad p_2 - q' + q_2, p_3 - q_2, p_4 - q_1\}, \end{aligned}$$

and

$$\tilde{s}_{14} = (p_1 + p_4 + q')^2, \quad \tilde{s}_{23} = (p_2 + p_3 - q')^2, \quad (54)$$

$$s_{ij} = (p_i + p_j)^2, \quad t_{1,2} = (p_{a,b} - p_{1,2})^2, \quad (55)$$

$$\hat{s} = (p_3 + p_4)^2, \quad \hat{t} = (p_a - p_1 - p_3)^2 \quad (56)$$

$$\begin{aligned} S_{h_1 h_2}(s, q^2) &= \int d^2 \vec{b} e^{i \vec{q} \vec{b}} (1 + 2i T_{h_1 h_2}^{el}(s, b)) = \\ &= \int d^2 \vec{b} e^{i \vec{q} \vec{b}} e^{-2\Omega_{h_1 h_2}^{el}(s, b)} = (2\pi)^2 \delta^2(\vec{q}) + 2\pi \bar{T}_{h_1 h_2}(s, q^2), \end{aligned}$$

$$\bar{T}_{h_1 h_2}(s, q^2) = \int_0^\infty b db J_0(b\sqrt{-q^2}) \left[e^{-2\Omega_{h_1 h_2}^{el}(s, b)} - 1 \right]$$

$$T_{h_1 h_2}^{el}(s, b) = \frac{e^{-2\Omega_{h_1 h_2}^{el}(s, b)} - 1}{2i},$$

$$\Omega_{h_1 h_2}^{el}(s, b) = -i \delta_{h_1 h_2}^{el}(s, b),$$

$$\delta_{h_1 h_2}^{el}(s, b) = \frac{1}{16\pi s} \int_0^\infty d(-t) J_0(b\sqrt{-t}) \delta_{h_1 h_2}^{el}(s, t)$$

$$\hat{F}_h = e^{(i-m_h^2)/\Lambda_h^2},$$

$$M_0^{C,\pi}(\{p\}) = T_{\pi^+ p}^{el}(s_{13}, t_1) \mathcal{P}_\pi(\hat{s}, \hat{t}) \left[\hat{F}_\pi(\hat{t}) \right]^2 T_{\pi^- p}^{el}(s_{24}, t_2),$$

$$\mathcal{P}_\pi(\hat{s}, \hat{t}) = \left(\text{ctg} \frac{\pi \alpha_\pi(\hat{t})}{2} - i \right) \cdot \frac{\pi \alpha'_\pi}{2 \Gamma(1 + \alpha_\pi(\hat{t}))} \left(\frac{\hat{s}}{s_0} \right)^{\alpha_\pi(\hat{t})},$$

$$\alpha_\pi(\hat{t}) = 0.7(\hat{t} - m_\pi^2)$$

$$M_0^{C,p}(\{p\}) = T_{pp}^{el}(s_{13}, t_1) \mathcal{P}_p(\hat{s}, \hat{t}) \left[\hat{F}_p(\hat{t}) \right]^2 T_{\bar{p}p}^{el}(s_{24}, t_2),$$

$$\mathcal{P}_p(\hat{t}) = \left(\text{ctg} \frac{\pi \alpha_\pi(\hat{t})}{2} - i \right) \cdot \frac{\pi \alpha'_\pi}{2 \Gamma(1 + \alpha_\pi(\hat{t}))} \left(\frac{\hat{s}}{s_0} \right)^{\alpha_\pi(\hat{t})},$$

$$\alpha_\pi(\hat{t}) = 0.7(\hat{t} - m_\pi^2)$$

$$V_{h_1 h_2}(s, q^2) = \int d^2 \vec{b} e^{i \vec{q} \vec{b}} \sqrt{1 + 2i T_{h_1 h_2}^{el}(s, b)} =$$

$$= \int d^2 \vec{b} e^{i \vec{q} \vec{b}} e^{-\Omega_{h_1 h_2}^{el}(s, b)} = (2\pi)^2 \delta^2(\vec{q}) + 2\pi \tilde{T}_{h_1 h_2}$$

$$\tilde{T}_{h_1 h_2} = \int_0^\infty b db J_0(b\sqrt{-q^2}) \left[e^{-\Omega_{h_1 h_2}^{el}(s, b)} - 1 \right]$$

References

1. R. Ryutin, *Exclusive Double Diffractive Events: general framework and prospects*, Eur. Phys. J. C. **73**, 2443 (2013).
2. R. Ryutin, *Visualizations of exclusive central diffraction*, Eur. Phys. J. C. **74**, 3162 (2014).
3. R. Ryutin, *Central exclusive diffractive production of two-pion continuum at hadron colliders*, Eur. Phys. J. C. **79**, 981 (2019).
4. V.A. Petrov, R.A. Ryutin, *Single and double diffractive dissociation and the problem of extraction of the proton-Pomeron cross-section*, Int. J. Mod. Phys. A **31**, 1650049 (2016).
5. J.D. Bjorken, *Rapidity gaps and jets as a new-physics signature in very-high-energy hadron-hadron collisions*, Phys. Rev. D **47**, 101 (1993).
6. F. Abe et al. (CDF Collaboration), *Observation of rapidity gaps in $\bar{p} p$ collisions at 1.8 TeV*, Phys. Rev. Lett. **74**, 855 (1995).
7. M.G. Albrow, A. Rostovtsev, *Searching for the Higgs at hadron colliders using the missing mass method*, FERMLAB-PUB-00-173 (2000), [arXiv: 0009336[hep-ph]].
8. L.A. Harland-Lang, V.A. Khoze, M.G. Ryskin, *Central exclusive production and the Durham model*, Int. J. Mod. Phys. A **29**, 1446004 (2014).
9. L.A. Harland-Lang, V.A. Khoze, M.G. Ryskin, W.J. Stirling, *Central exclusive production within the Durham model: a review*, Int. J. Mod. Phys. A **29**, 1430031 (2014).
10. L.A. Harland-Lang, V.A. Khoze, M.G. Ryskin, *Modeling exclusive meson pair production at hadron colliders*, Eur. Phys. J. C **74**, 2848 (2014).
11. P. Lebiedowicz, O. Nachtmann, A. Szczurek, *Tensor pomeron, vector odderon and diffractive production of meson and baryon pairs in proton-proton collisions*, EPJ Web Conf. **206**, 06005 (2019).
12. P. Lebiedowicz, O. Nachtmann, A. Szczurek, *Exclusive diffractive production of $\pi^+ \pi^-$ continuum and resonances within tensor pomeron approach*, EPJ Web Conf. **130**, 05011 (2016).
13. P. Lebiedowicz, O. Nachtmann, A. Szczurek, *Central exclusive diffractive production of $K^+ K^- K^+ K^-$ via the intermediate $\phi\phi$ state in proton-proton collisions*, Phys. Rev. D **99**, 094034 (2019).
14. C. Ewerz, M. Maniatis, O. Nachtmann, *A Model for Soft High-Energy Scattering: Tensor Pomeron and Vector Odderon*, Ann. of Phys. **342**, 31 (2014); [arXiv:1309.3478 [hep-ph]].
15. P. Lebiedowicz, O. Nachtmann, A. Szczurek, *Central exclusive diffractive production of $\pi^+ \pi^-$ continuum, scalar and tensor resonances in pp and $p\bar{p}$ scattering within tensor pomeron approach*, Phys. Rev. D **93**, 054015 (2016); [arXiv:1601.04537 [hep-ph]].
16. P. Lebiedowicz, O. Nachtmann, A. Szczurek, *Extracting the pomeron-pomeron- $f_2(1270)$ coupling in the $pp \rightarrow pp\pi^+ \pi^-$ reaction through angular distributions of the pions*, Phys. Rev. D **101**, 034008 (2020); [arXiv:1901.07788 [hep-ph]].
17. P. Lebiedowicz, O. Nachtmann and A. Szczurek, *ρ_0 and Drell-Soding contributions to central exclusive production of $\pi^+ \pi^-$ pairs in proton-proton collisions at high energies*, Phys. Rev. D **91**, 074023 (2015); [arXiv:1412.3677 [hep-ph]].
18. P. Lebiedowicz, A. Szczurek, *Revised model of absorption corrections for the $pp \rightarrow p\pi^+ \pi^- p$ process*, Phys. Rev. D **92**, 054001 (2015).
19. R. Waldi, K.R. Schubert and K. Winter, *Search for glueballs in a pomeron pomeron scattering experiment*, Z. Phys. C **18**, 301 (1983).

20. A. Breakstone et al. (ABCDHW Collaboration), *The reaction Pomeron-Pomeron $\rightarrow \pi^+\pi^-$ and an unusual production mechanism for the $f_2(1270)$* , Z. Phys. C **48**, 569 (1990).
21. L. Adamczyk, W. Guryn and J. Turnau, *Central exclusive production at RHIC*, Int. J. Mod. Phys. A **29**, 1446010 (2014).
22. R. Sikora, *Central Exclusive Production of meson pairs in proton-proton collisions at $\sqrt{s} = 200$ GeV in the STAR experiment at RHIC*, talk at Low x Meeting, 1-5 September 2015, Sandomierz, Poland.
23. J. Adam et al. (The STAR collaboration), *Measurement of the central exclusive production of charged particle pairs in proton-proton collisions at $\sqrt{s} = 200$ GeV with the STAR detector at RHIC*, JHEP **07**, 178 (2020); [arXiv:2004.11078 [hep-ex]]; <https://www.hepdata.net/record/ins1792394>
24. W. Guryn, *From Elastic Scattering to Central Exclusive Production: Physics with Forward Protons at RHIC*, Acta Phys. Pol. B **52**, 217 (2021); [arXiv:2104.15041 [nucl-ex]].
25. R. Sikora (for the STAR Collaboration), *Central exclusive production of charged particle pairs in proton-proton collisions at $\sqrt{s} = 200$ GeV with the STAR detector at RHIC*, PoS **ICHEP2020**,501 (2021); [arXiv:2011.14400 [hep-ex]]
26. T. Truhlar (for the STAR Collaboration), *Study of the central exclusive production of $\pi^+\pi^-$, K^+K^- and $p\bar{p}$ pairs in proton-proton collisions at $\sqrt{s} = 510$ GeV with the STAR detector at RHIC*, [arXiv:2012.06295 [hep-ex]].
27. T.A. Aaltonen et al. (CDF Collaboration), *Measurement of central exclusive $\pi^+\pi^-$ production in $p\bar{p}$ collisions at $\sqrt{s} = 0.9$ and 1.96 TeV at CDF*, Phys. Rev. D **91**, 091101 (2015).
28. M. Albrow, J. Lewis, M. Zurek, A. Swiech, D. Lonkowskyi, I. Makarenko and J.S. Wilson, the public note called *Measurement of Central Exclusive Hadron Pair Production in CDF* is available at http://www-cdf.fnal.gov/physics/new/qcd/GXG_14/webpage/.
29. CMS Collaboration, *Measurement of exclusive $\pi^+\pi^-$ production in proton-proton collisions at $\sqrt{s} = 7$ TeV*, CMS-PAS-FSQ-12-004.
30. K. Osterberg, *Potential of central exclusive production studies in high β^* runs at the LHC with CMS-TOTEM*, Int. J. Mod. Phys. A **29** 1446019 (2014).
31. A.M. Sirunyan et al., *Study of central exclusive $\pi^+\pi^-$ production in proton-proton collisions at $\sqrt{s} = 5.02$ and 13 TeV*, Eur. Phys. J. C **80**, 718 (2020); <https://www.hepdata.net/record/ins1784063>
32. A.A. Godizov, *Effective transverse radius of nucleon in high-energy elastic diffractive scattering*, Eur. Phys. J. C **75**, 224 (2015).
33. A.A. Godizov, *Asymptotic properties of Regge trajectories and elastic pseudoscalar-meson scattering on nucleons at high energies*, Yad. Fiz. **71**, 1822 (2008).
34. A.A. Godizov, *The ground state of the Pomeron and its decays to light mesons and photons*, Eur. Phys. J. C **76**, 361 (2016); [arXiv:1604.01689 [hep-ph]].
35. J.R. Pelaez, A. Rodas, J. Ruiz De Elvira, *Global parameterization of $\pi\pi$ scattering up to 2 GeV*, e-Print: arXiv:1907.13162 [hep-ph].
36. A.A. Godizov, *Current stage of understanding and description of hadronic elastic diffraction*, AIP Conf.Proc. **1523**, 145 (2013).
37. V.A. Petrov, R.A. Ryutin, A.E. Sobol and J.-P. Guillaud, *Azimuthal angular distributions in EDDE as spin-parity analyser and glueball filter for LHC*, JHEP **0506**, 007 (2005).
38. V.A. Petrov, *High-energy implications of extended unitarity*, IFVE-95-96, IHEP-95-96, talk given at Blois Conference: 20-24 Jun 1995, Blois, France
39. A.A. Godizov, *High-energy central exclusive production of the lightest vacuum resonance related to the soft Pomeron*, Phys. Lett. B **787**, 188 (2018).
40. R.A. Ryutin, *ExDiff Monte Carlo generator for Exclusive Diffraction. Version 2.0. Physics and manual*, [arXiv:1805.08591 [hep-ph]].